J Mater Sci (2008) 43:2–11
DOI 10.1007/s10853-007-1791-7

JOINING SCIENCE & TECHNOLOGY

Local melting and tool slippage during friction stir spot welding of Al-alloys

Adrian Gerlich · Motomichi Yamamoto · Thomas H. North

Received: 13 March 2007 / Accepted: 18 April 2007 / Published online: 15 November 2007

Abstract Local melting and tool slippage during friction stir spot welding of different Al-alloy base materials is examined using a combination of detailed microscopy and temperature measurement. The stir zone peak temperature during welding is limited by either the solidus of the alloy in question or by spontaneous melting of intermetallic particles contained in the as-received base material. When spontaneous melting occurs this facilitates tool slippage at the contact interface. Accurate stir zone temperature and grain size measurements are essential elements when estimating the strain rate using the Zener–Hollomon relation. In Al 2024 and Al 7075 spot welds spontaneous melting of second-phase particles produces a drastic reduction in strain rate values. In Al 5754 and Al 6061 spot welds there is a strong correlation between tool rotational speed and estimated strain values. Local melted films dissolve rapidly in the high temperature stir zone and when the spot weld cools to room temperature following welding. Evidence of local melting is observed in Al 7075 friction stir spot welded joints made using a combination of rapid quenching, high plunge rates, and extremely short dwell time settings.

Introduction

The friction stir welding process was developed by TWI, Abington, UK in 1991 for joining aluminum alloys [1]. During friction stir welding a joint is made between contacting sheets by traversing a rotating tool comprising a pin and shoulder between the mating surfaces. Dynamically recrystallized material formed adjacent to the periphery of the rotating tool creates a weld between the contacting work pieces.

During friction stir spot welding a rotating tool is plunged into and out of two overlapping sheets at a single location. When the pin penetrates into the contacting sheets, a stir zone is formed comprising dynamically recrystallized material and a keyhole region is left in the welded component when the rotating tool is retracted. The keyhole can be filled via the use of a specially-designed tool fixture if desired [2]. The tool penetration process and the factors determining weld mechanical properties have been investigated during spot welding of Al- and Mg-alloy sheet materials [3–6].

Energy generation resulting from viscous dissipation during friction stir welding is ultimately limited by either tool slippage or the attainment of the solidus temperature of the alloy being fabricated [3, 7–13]. For example, North et al. [14] proposed that local melting and tool slippage could account for the low travel speeds that are obtainable during friction stir seam welding of Al 2024 and Al 7075 sheets. Gerlich et al. [7, 8] provided support for this proposal in detailed investigations of Al 2024 and Al 7075 friction stir spot welding. The remarkable decrease in estimated strain rate values in spot welds made using high tool rotational speed settings was associated with spontaneous melting of second-phase particles (η, S, and T phases), which promoted tool slippage at the contact interface between the periphery of the rotating tool and adjacent material in the stir zone. High tool rotational speed settings produced a combination of high heating rate and high stir zone temperature, which facilitated local melting and tool slippage during friction stir spot welding.

A. Gerlich (✉) · M. Yamamoto · T. H. North
Department of Materials Science & Engineering, University of Toronto, 184 College St., Rm. 140, Toronto, ON, Canada M5S 3E4
e-mail: gerlich@ecf.utoronto.ca

It must be emphasized that local melting and tool slippage are not characteristic features when all Al-alloys are fabricated using friction stir spot welding. For example, it has been recently confirmed that local melting and tool slippage do not occur during Al 5754 and Al 6061 friction stir spot welding since second-phase particles having melting points less than their respective solidus temperatures are not present [15]. As a result, much higher strain rates are produced in the contact region between the periphery of the rotating tool and adjoining stir zone material during Al 5754 and Al 6061 friction stir spot welding.

Experimental evidence supporting local melting during friction stir welding and friction stir spot welding has been provided by a number of investigators. For example, local melted films have been observed in Al 2024-T3 friction stir welds [16], in Al 6061-T6 Al_2O_3 plunge tests [17], in AZ31 spot welds [13], in dissimilar Al 6111/AZ91 spot welds [11], and in dissimilar Al 1050/AZ31 friction stir welds [18]. In spite of this experimental output, transient local melting remains a remarkably controversial issue.

The present article investigates local melting and tool slippage during friction stir spot welding of Al-alloy base materials. Tool slippage during friction stir spot welding is investigated by incorporating EBSD microstructural output and stir zone temperature measurements into the Zener–Hollomon relation. The critical aspects of strain rate estimation are outlined, including the demands for accurate stir zone temperature and grain size measurements.

Experimental

Table 1 shows the chemical compositions of the Al-alloy base materials that were examined. Spot welds were produced in 1.5 mm thick overlapping sheets and in 6 mm plate.

The tool geometry comprised a 10 mm diameter shoulder, a pin diameter of 4 mm, and a pin length of 2.2 mm. The rotating pin had a simple threaded profile. The tool comprised H13 steel (0.35 wt.% C, 5 wt.% Cr, 1.5 wt.% Mo, 1 wt.% V), heat-treated and tempered to a final hardness of 46–48 HRC. A plunge rate of 2.5 mm/s was used during all spot welding temperature measurements, while the specified pin penetration depth was 2.2 mm. This penetration depth corresponds with the point when the tool shoulder just contacts the upper surface of the sheet being spot welded. When the rotating pin was fully-penetrated the spot welding cycle was extended by incorporating a dwell time of 4 s. The tool rotational speed remained constant while axial force and torque decreased during the 4-s long dwell period and due to machine compliance, the rotating tool penetrated up to 200 μm into the upper surface of the Al-alloy section.

The influence of tool rotational speed variations from 750 to 3,000 RPM on the average subgrain dimensions and temperatures in the stir zone was investigated. Since almost all of the energy generated during friction stir spot welding is due to the torque resulting from tool rotation [9], stir zones made using rotational speeds $\leq$750 RPM did not have bonded regions having acceptable dimensions and joint mechanical properties [7, 8]. With this in mind, the welding parameters used the present investigation are those that produced stir zones having widths >100 μm.

The thermal cycle during friction stir spot welding was measured by embedding 0.25 mm diameter K-type thermocouples at the location 0.2 mm from the tip of the rotating pin and 1.3 mm from the outer periphery of the tool shoulder, see Fig. 1. During all temperature measurements the thermocouple junction was always in direct contact with dynamically recrystallized material formed during the spot welding operation. A detailed description of the temperature measurement set-up has been provided elsewhere [7]. All temperature measurements were repeated at least three times at each welding parameter setting. The variation in temperature during the 4-s dwell period was <7.4 °C during repeat testing. The error bars shown on any figure indicate one standard deviation above and below the reported value.

During optical microscopy the test samples were polished using 1 μm diamond compound and then etched using Kelller's reagent prior to viewing in normal light. Test samples were also electrolytically etched at 30 V with 3% HBF_4 for 2 min and viewed using polarized light microscopy.

Electron backscattered diffraction (EBSD) was used to obtain detailed quantitative information concerning the stir zone microstructure. The surface of each sample was

Table 1 Base material compositions, in wt%

Alloy	Al	Cr	Cu	Fe	Mg	Mn	Si	Ti	Zn
Al 2024-T3	bal.	<0.01	4.30	0.15	1.42	0.62	0.07	0.03	0.07
Al 5754-O	bal.	0.02	0.01	0.21	3.08	0.26	0.08	<0.01	0.02
Al 6061-T6	bal.	0.08	0.19	0.19	0.82	0.02	0.49	0.01	<0.01
Al 7075-T6	bal.	0.21	1.27	0.12	2.34	<0.01	0.07	<0.01	5.41

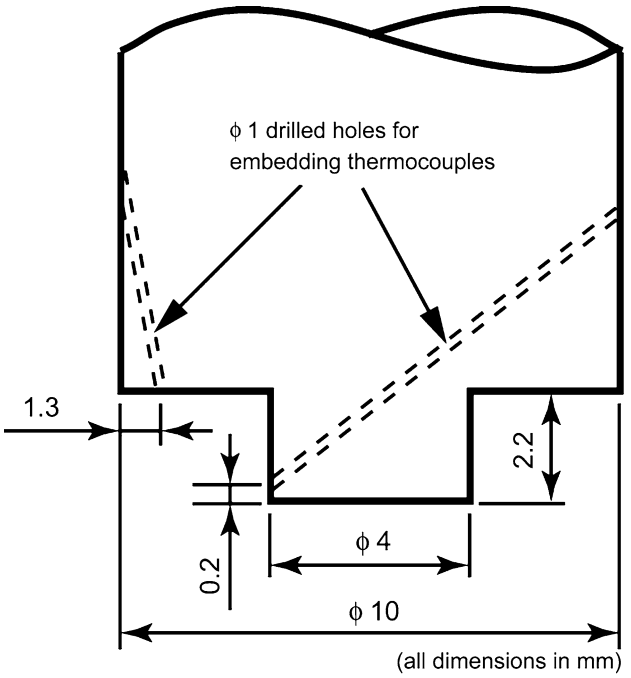

Fig. 1 Thermocouple locations within the tool itself; all dimensions in mm

ground using 1,200 grit SiC prior to EBSD examination and final electro-polishing was carried out using a solution of 25 vol.% of HNO_3 and 75 vol.% of methanol at a temperature of −30 °C and a voltage of 12 V. The step size was 0.2–0.3 μm during EBSD while the angular resolution limit of the equipment was about 1.5°. The grain boundary statistics were determined using a Hitachi S-4500 field emission scanning electron microscope having HKL Channel5 software. At least five points per grain were indexed in the EBSD scan and the remaining non-indexed points were interpolated using a clean-up algorithm, which averaged the missing data with the three nearest neighbors. Spot welds were rapidly quenched in a mixture of methanol and liquid nitrogen at a temperature of −80 °C immediately following tool retraction.

Results and discussion

Stir zone temperature

The pin temperature and power input during spot welding of Al 2024 sections are shown in Fig. 2. During the plunge period (from 0 to 1.3 s) the tool pin undergoes rapid heating. Although the power input decreases during the dwell period in spot welding (from 1.3 to 5.3 s), the pin temperature increases gradually. Since the stir zone volume determined from metallographic cross-sections is approximately 50–100 mm^3, the power density is extremely high

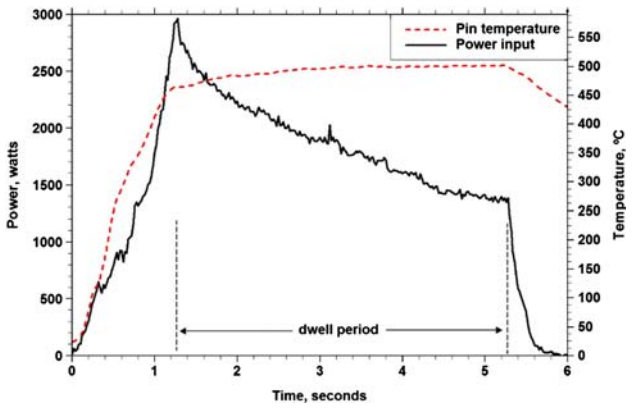

Fig. 2 Power input and the measured temperature 0.2 mm from the tip of the rotating pin in Al 2024 spot welds made using a tool rotational speed of 3,000 RPM

(around 10^{10} W/m^3) during friction stir spot welding. The efficiency of heat transfer is close to 100% during friction stir spot welding since only a small percentage of the energy, which is generated during tool rotation is required for stir zone formation [9, 10]. Much of the energy generated during the friction stir spot welding operation is transferred in the available heat sinks (into the tool assembly, the steel anvil beneath the test samples, the holding clamp, and the adjoining sheets). This readily explains why the solidus temperature is approached the stir zone when Al-alloy or Mg-alloy sections are fabricated. For example, the highest temperatures found in the stir zones of Al 2024, Al 5754, Al 6111, Al 6061, Al 7075, AZ31, AZ91, and AM50 alloy friction stir spot welds correspond with homologous temperatures ranging from 0.94 to 0.99 [3, 6–13, 15]. This experimental testing output provides strong support for the proposal made by Bendzsak et al. [19] and North et al. [14] that the peak temperature during friction stir welding approaches the solidus temperature of the base material being welded.

The heating rate during the tool penetration stage in friction stir spot welding is determined by the tool rotational speed employed (see Fig. 3). However, the high heating rate produced during friction stir spot welding is important from a quite different perspective. Since the heating rate ranges from 210 to 400 °C/s during spot welding, second-phase particles contained in the as-received base material have insufficient time to dissolve and melt spontaneously when their melting temperatures are attained. The η, S, and T particles contained in as-received Al 7075-T6 base material, for example, melt spontaneously when the stir zone temperature reaches 475, 480 and 490 °C [20–22]. It has been suggested that spontaneous melting of second-phase particles produces tool slippage at the contact interface between the periphery of the rotating tool and adjacent material in the stir zones of

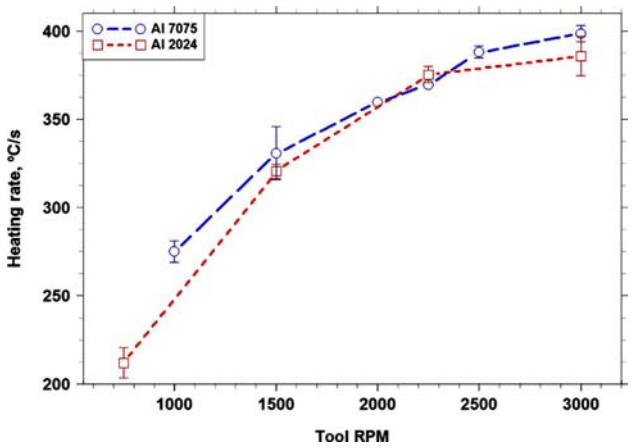

Fig. 3 Influence of tool rotational speed on the heating rates during Al 2024 and Al 7075 friction stir spot welding

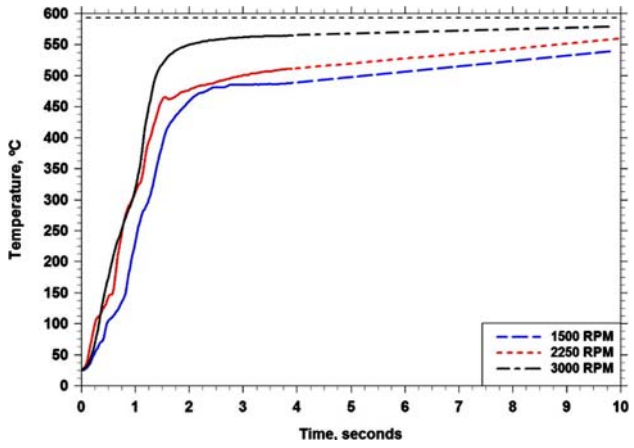

Fig. 4 Measured temperatures in the location 0.2 mm from the tip of the rotating pin during friction stir spot welding of Al 5754 using tool rotational speeds from 1,500 to 3,000 RPM. Temperature values beyond a dwell time of 4 s have been extrapolated to 10 s (see the dashed lines in the above figure)

Al 7075-T6 and Al 2024-T3 [7, 8]. Also, fluctuations in the measured temperature during the dwell period in Al 7075-T6 spot welding have been associated with spontaneous melting of second-phase particles since spontaneous melting is immediately followed by solidification of liquid droplets, which increases the material viscosity, heating rate, and temperature prior to reformation of liquid droplets [7].

The heating rate also determines the peak temperature, which is attained early in the dwell period. Figure 4 shows that the temperature at the beginning of the dwell period during Al 5754 spot welding is determined by the tool rotational speed setting. When the results produced during a 4-s dwell period are extrapolated to 10 s the peak temperature approaches the solidus temperature of Al 5754 at all tool rotational speed settings. Similar behavior is observed during Al 2024, Al 6061, and Al 7075 friction stir spot welding [23].

During Al 2024 and Al 7075 spot welding using a tool rotational speed of 3,000 RPM the peak temperature at end of the plunging stage is limited by tool slippage resulting from spontaneous melting of η, S, and T particles. The reported solidus temperatures of Al 2024 and well-homogenized Al 7075 are 502 and 532 °C [24]. These solidus temperatures are approached when the dwell period is extended to 4 s since second-phase particles are rapidly dissolved [7, 8] and the amount of material incorporated into the stir zone decreases [25]. The highest temperatures in Al 2024 and Al 7075 spot welds made using a dwell time of 4 s correspond with a homologous temperature 0.99 (see Fig. 5a). Al 5754 and Al 6061 have solidus temperatures of 590 °C [26] and 582 °C [27], and the highest temperatures during Al 5754 and Al 6061 friction stir spot welding correspond with a homologous temperature of 0.95 (see Fig. 5b).

It is remarkably difficult to obtain satisfactory temperature output during friction stir seam and friction stir spot welding operations. For example, it has been recently found that the stir zone temperature in friction stir spot welds cannot be determined by embedding thermocouples in drilled holes within 0.5 mm from the periphery of the rotating pin prior to spot welding since the helical vertical rotational flow set-up within the stir zone formed adjacent to the periphery of the rotating pin displaces thermocouples from their original locations [25]. The most effective means of measuring temperature during friction stir spot

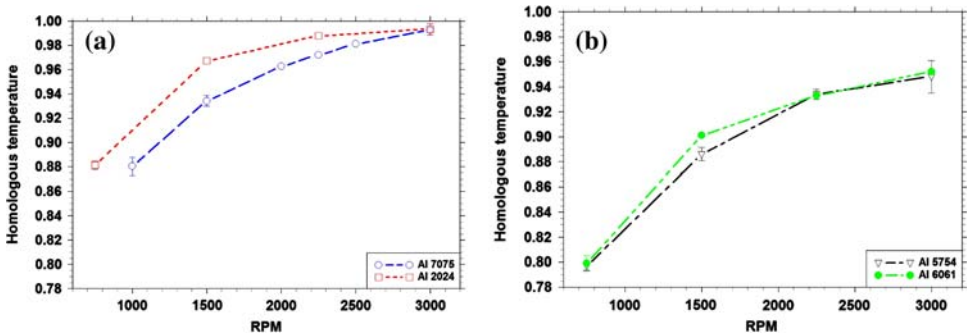

Fig. 5 Stir zone temperature and tool rotational speed relations during (**a**) Al 2024 and Al 7075 spot welding, and (**b**) Al 5754 and Al 6061 spot welding

welding is by locating the thermocouples within the tool itself (see Fig. 1). However, even when this methodology is employed, the measured temperature values are likely less than the actual temperatures at the contact interface. Also, a steep temperature gradient exists immediately adjacent to a frictionally heated contact surface and the temperature decreases markedly at small distances from the interface [19, 28–31]. In this connection, although the temperature in the TMAZ region can be measured by embedding thermocouples into test samples prior to spot welding it is particularly difficult to obtain consistent temperature output at a *pre-selected location* relative to the stir zone extremity [32].

The problems encountered when measuring temperature by embedding thermocouples in drilled holes in the component prior to friction stir spot welding are exacerbated when friction stir seam welding is involved. The difficulties encountered in measuring the temperature at particular locations within the stir zone and TMAZ by embedding thermocouples in drilled holes ahead of the traversing tool are much increased and this may well explain the remarkable scatter in reported temperature values during friction stir seam welding operations [33, 34]. Also, since the stir zone temperature cannot be measured by embedding thermocouples in the component prior to friction stir spot welding, it is difficult to visualize how the temperature in the nugget region can be measured when thermocouples are embedded ahead of the traversing tool during friction stir seam welding. With this in mind, the reported stir zone temperature values found by embedding thermocouples in drilled holes ahead of the traversing tool during friction stir seam welding are at best doubtful. In this connection, there has been much discussion whether there is a temperature difference between the advancing and retreating sides of friction stir seam welds [34, 35]. It is apparent from the above commentary that the application of a measuring technique that involves embedding thermocouples ahead of the traversing tool will not answer this particular question.

Stir zone microstructure

Figure 6a shows an optical micrograph of a typical Al 7075 friction stir spot welding produced using a tool rotational speed of 3,000 RPM. Region I, located 100 μm from the keyhole periphery halfway up the length of the rotating pin, was examined using EBSD. Figure 6b and c shows details of the stir zones produced when dwell times of 1 and 4 s are applied.

Typical EBSD misorientation maps from Region I in rapidly-quenched Al 2024, Al 7075, Al 5754, and Al 6061 spot welds produced using a tool rotational speed of 3,000 RPM are shown in Fig. 7. The average grain size values were calculated from misorientation maps using the linear intercept method, with only grain boundaries having >2° misorientations considered. At least two locations in repeated test welds were examined and provided a minimum of 400 intercept measurements for each welding condition. Table 2 shows the average EBSD grain size estimates in Region I when examining Al 2024, Al 7075, Al 5754, and Al 6061 spot welds produced using different tool rotational speed settings. The error ranges indicated in Table 2 are quite narrow since a large number of boundary intercepts are included in the calculated average values.

A fine-grained dynamically-recrystallized microstructure is formed in the stir zone. Figure 8 shows the EBSD grain size distribution across the stir zone width in Al 2024, Al 7075, Al 5754, and Al 6061 spot welds made using a tool rotational speed of 3,000 RPM. The grain size is nearly uniform up to 200 μm from the keyhole; this location corresponds with Region I in Fig. 6a.

Mishin et al. recently compared the quantitative output produced when the stir zone microstructure in friction stir seam welds was examined using EBSD and TEM microscopy [36]. The estimated grain size using EBSD depended on the boundary criteria used and corresponded with the values found using TEM microscopy when a 2° misorientation criteria was applied. Also, the step size during EBSD analysis must be small enough to measure individual grains. Humphreys has already pointed out that EBSD produces average grain size values, which are within 10% of those found using TEM microscopy provided that at least 5 pixels per grain are captured [37].

The grain size estimates in Table 2 are based on detailed TEM and EBSD microscopy, with a 2° misorientation criterion applied [7, 8, 38]. In this connection, Region I is much easier to examine using EBSD because of specimen extraction problems during TEM. Since the grain size increases at distances >200 μm from the keyhole periphery (see Fig. 8), increased scatter will result when TEM foils are not extracted with considerable care.

Strain rate during friction stir spot welding

During high temperature deformation the strain rate and temperature are related as follows:

$$Z = \dot{\varepsilon}\exp\left(\frac{Q}{RT}\right), \tag{1}$$

where Z is the Zener–Hollomon parameter (the temperature compensated strain rate), $\dot{\varepsilon}$ is the strain rate, T is the deformation temperature, Q is the activation energy and R is the universal gas constant [39]. In wrought aluminum alloys and austenitic stainless steels, the Zener–Hollomon

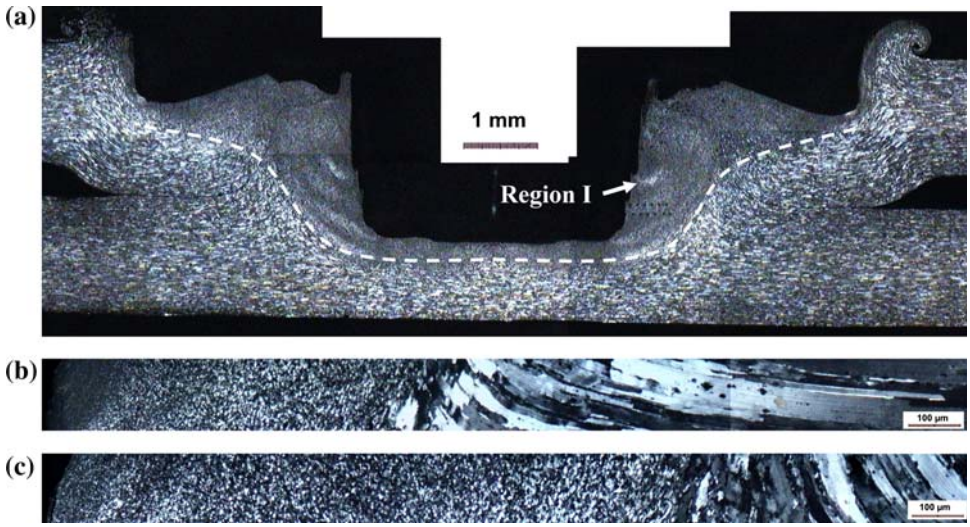

Fig. 6 (**a**) Polarized light micrograph of Al 7075 friction stir spot welds made using a rotational speed of 3,000 RPM and a dwell time of 4 s. The boundary of stir zone is demarcated by the dashed line. Region I shows the location examined using electron microscopy, (**b**) Detail of Region I when a dwell time of 1 s is applied, and (**c**) Detail of Region I when a dwell time of 4 s is applied

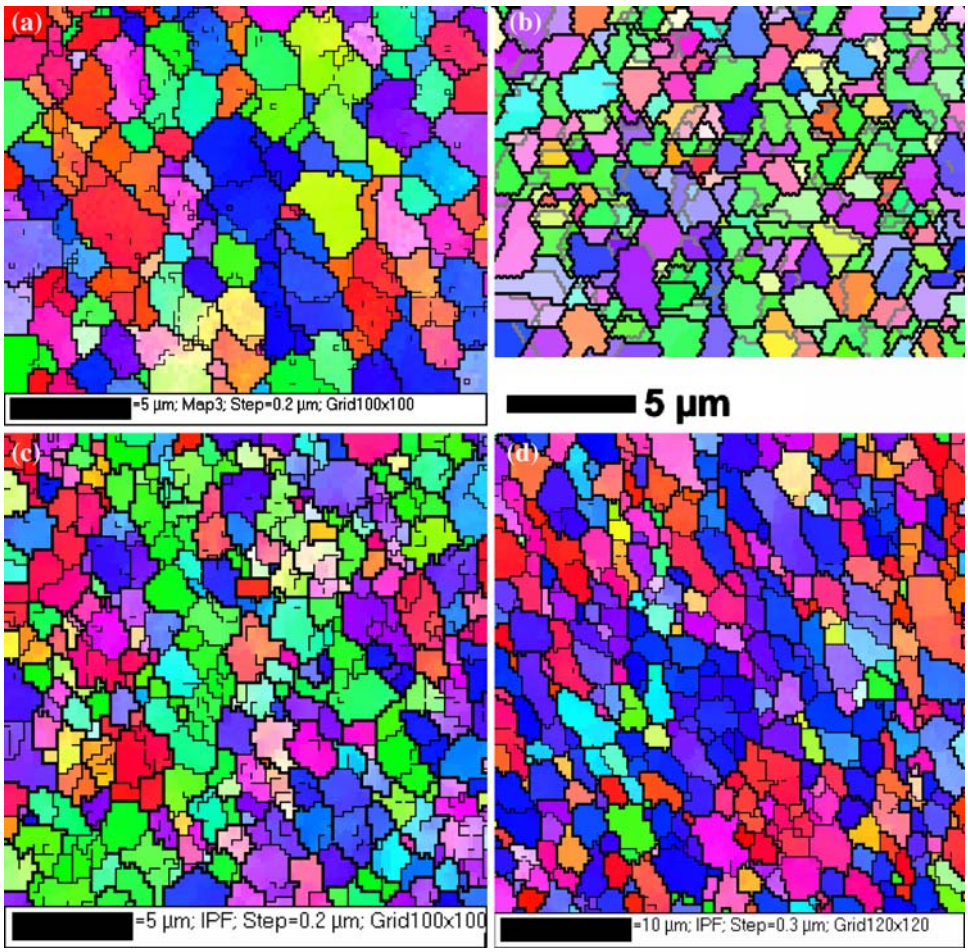

Fig. 7 EBSD maps of the stir zone Region I located at a distance of 100 μm from keyhole periphery in (**a**) Al 2024, (**b**) Al 7075, (**c**) Al 5754, and (**d**) Al 6061 friction stir spot welds, produced using 3,000 RPM and a dwell time of 4 s

parameter and the subgrain diameter, d, are related as follows [40–45]:

$$d^{-1} = a + b\log(Z), \tag{2}$$

where a and b are constitutive constants. Equations 1 and 2 provide a ready means of estimating the strain rate during friction stir spot welding provided that accurate values for the average subgrain dimensions and the deformation temperatures are available.

The strain rates during Al-alloy friction stir spot welding were determined using the average grain sizes found by EBSD (see Table 2) and the stir zone temperatures

Table 2 Summary of EBSD stir zone grain sizes (in μm) within Region I

RPM	Al 2024	RPM	Al 7075	RPM	Al 5754	RPM	Al 6061
750	0.57 ± 0.02	1,000	0.68 ± 0.08	750	1.10 ± 0.09	750	1.05 ± 0.16
1,500	0.80 ± 0.06	1,500	0.95 ± 0.10	1,500	1.40 ± 0.19	1,500	1.41 ± 0.16
2,250	0.87 ± 0.09	2,250	1.08 ± 0.05	2,250	1.49 ± 0.21	2,250	1.73 ± 0.13
3,000	1.23 ± 0.21	3,000	1.86 ± 0.16	3,000	1.51 ± 0.16	3,000	2.09 ± 0.18

Error ranges correspond with one standard deviation above and below the mean value

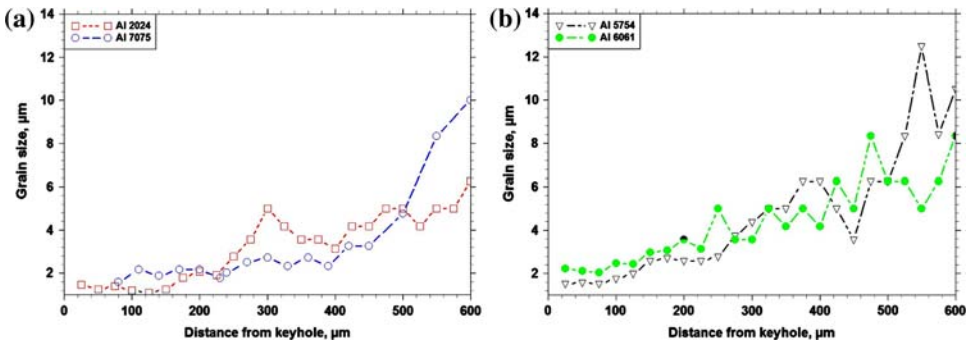

Fig. 8 EBSD grain size distributions across stir zone in (**a**) Al 2024 and Al 7075, and (**b**) Al 5754 and Al 6061 spot welds produced using a tool rotational speed of 3,000 RPM and a dwell time of 4 s

indicated in Fig. 5. The constitutive constants in Eqs. 1 and 2 correspond with those determined during torsion testing of each Al-alloy base material, see Table 3. For example, in the case of Al 7075, the constitutive constants are obtained directly from the high temperature torsion output produced by Cerri et al. [43] and Sheppard [44]. When the material constants Q, a, and b are not available for a particular alloy, the values for an Al-alloy having a similar chemical composition are substituted instead. In the case of the Al 2024, the constants for Al 2014 alloy were applied [46]. Figure 9a shows the relation between the calculated strain rate and the rotational speed during Al 2024 and Al 7075 spot welding. The calculated strain rate decreased from 1,600 and 650 s^{-1} to about 20 s^{-1} when the tool rotational speed increased from 750 to 3,000 RPM during Al 7075 spot welding. The dramatic decrease in the calculated strain rate is indicative of tool slippage occurring during welding.

Figure 9b shows the estimated strain rates during Al 5754 and Al 6061 friction stir spot welding [15]. There is a strong positive correlation between the estimated strain rate values and the tool rotational speed. The strain rates for Al 5754 were calculated using material constants for alloy Al 5083 [47] while the strain rates for Al 6061 spot welds were calculated using material constants calculated directly from Zener–Hollomon parameter vs. grain size test results for Al 6061 and Al 6060 alloys [48, 49]. It should be noted that in the case of Al 6061 friction stir spot welding, rapid quenching is essential in determining the strain rate since grain growth occurs as the weld cools to room temperature [15].

Although the constants shown in Table 3 may not be exact values for the Al-alloys in question, the trends in the strain rate versus tool rotational speed relations (Fig. 9) will not be markedly altered. It is the overall trend between estimated strain rate values and tool rotational speed, which is important. The rate of heat generation during welding will depend on whether a slip or a no-slip boundary condition exists at the tool interface. Determining whether tool slippage does or does not occur is an essential element during numerically modeling of the friction stir spot welding process.

It has been suggested recently that the helical vertical rotational flow established within the stir zone during the dwell period in spot welding creates a uniform temperature across the width of the stir zone [25]. Assuming that the bulk of the stir zone has a similar temperature to that measured at the location 0.2 mm from the tip of the rotating pin, the change in strain rate across the stir zone can be calculated using the average grain size dimensions shown in Fig. 10. It is worth noting that if a modest temperature gradient of 50 °C/mm did exist across the stir zone, this would produce a negligible effect on the calculated strain rates away shown in Fig. 10. The strain rate distributions across the stir zones in Al 2024 and Al 7075

Table 3 Material constants for Eqs. 1 and 2

Alloy	Q (kJ/mol)	a	b
Al 2024	144	1.095	0.087
Al 5754	163	1.42	0.159
Al 6061	156	1.75	0.244
Al 7075	143	3.43	0.162

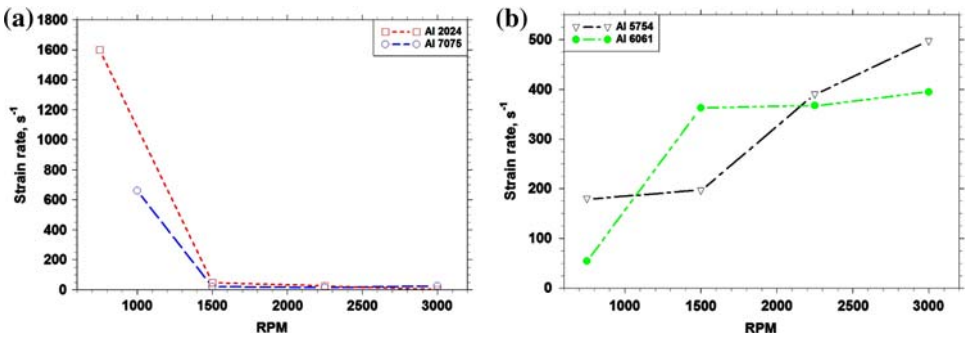

Fig. 9 Relation between the estimated strain rate and tool rotational speed in (**a**) Al 2024 and Al 7075 friction stir spot welds, and (**b**) Al 5754 and Al 6061 friction stir spot welds

spot welds are shown in Fig. 10a while those in Al 5754 and Al 6061 spot welds are shown in Fig. 10b.

It is apparent from Fig. 10b that the highest strain rate values in Al 5754 and Al 6061 friction stir spot welds (200–450 s^{-1}) occur within a distance of 200 μm from the tool periphery. These results are consistent with the no slip proposal recently made by Gerlich et al. [15] when examining Al 5754 and Al 6061 spot welds. Since much of the energy resulting from viscous dissipation during friction stir spot welding is generated in the region close to the periphery of the rotating tool and this particular region has a volume, which is much less than the volume of the stir zone this suggests that the apparent power densities during Al 5754 and Al 6061 friction stir spot welding are much higher than the value indicated earlier in this article (10^{10} W/m^3).

The estimated strain rates during Al 7075 and Al 2024 spot welding are much lower than those in Al 5754 and Al 6061 spot welds since tool slippage occurs at the contact interface between the tool periphery and adjacent material in the stir zone. Tool slippage results in strain rates values less than 30 s^{-1} across the width of the stir zones formed during Al 7075 and Al 2024 spot welding (see Fig. 10a). Bearing in mind the scatter in average grain size values measured using EBSD it could be argued that the average grain size in the location within 200 μm of the keyhole periphery in Al 7075 spot welds is almost constant (see Fig. 8). As a result, the strain rate is not markedly changed across the width of the stir zone in Al 2024 and Al 7075 friction stir spot welds.

Local melting

The low estimated strain rate values during Al 7075 and Al 2024 friction stir spot welding (see Fig. 9a) have been associated with spontaneous melting of second-phase η, S, and T phases [7, 8]. However, as mentioned earlier in this article the proposition that transient local melting occurs during friction stir welding is a remarkably controversial and contentious issue. For example, although the low strain rate values found during Al 7075 and Al 2024 spot welding are consistent with a local melting proposition, finding supporting metallographic evidence is the key issue. For example, the voids that Gerlich et al. [7, 8] observed on TEM specimens extracted from the stir zones of Al 7075 and Al 2024 spot welds may be due to (i) preferential etching of eutectic-rich regions at grain boundaries or (ii) artifacts created during TEM foil preparation (see Fig. 11). The need for supporting metallographic evidence remains in spite of the fact that detailed calculations indicate that local melted droplets formed during spot welding would completely dissolve in the high temperature stir zone and as spot welds cool to room temperature [7, 8].

Figure 12 shows an SEM micrograph of the location immediately beneath the tool shoulder in a rapidly-quenched Al 7075 spot weld made using a tool rotational speed of 3,000 RPM, a plunge rate of 10 mm/s and an extremely short dwell time (0.05 s). The local melted eutectic films shown in Fig. 12 are etched preferentially and are rich in Zn and Cu. In this connection, the formation of Cu- and Mg-rich films at grain boundary regions has already been

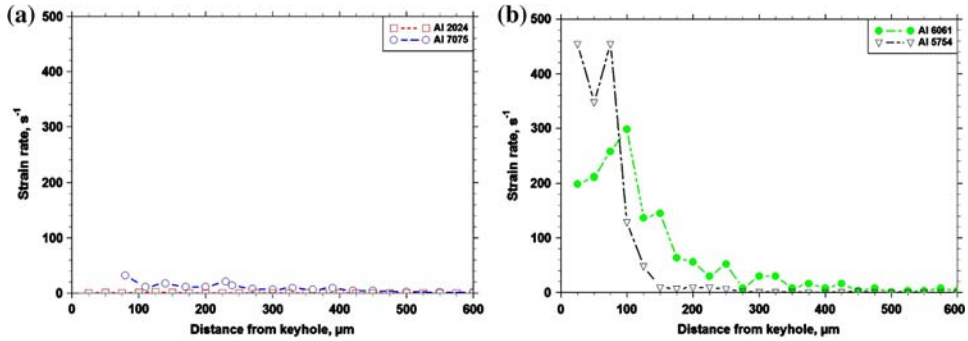

Fig. 10 Calculated strain rate distributions across the width of the stir zones in (**a**) Al 2024 and Al 7075, and (**b**) Al 5754 and Al 6061 spot welds produced using a tool rotational speed of 3,000 RPM and a dwell time of 4 s

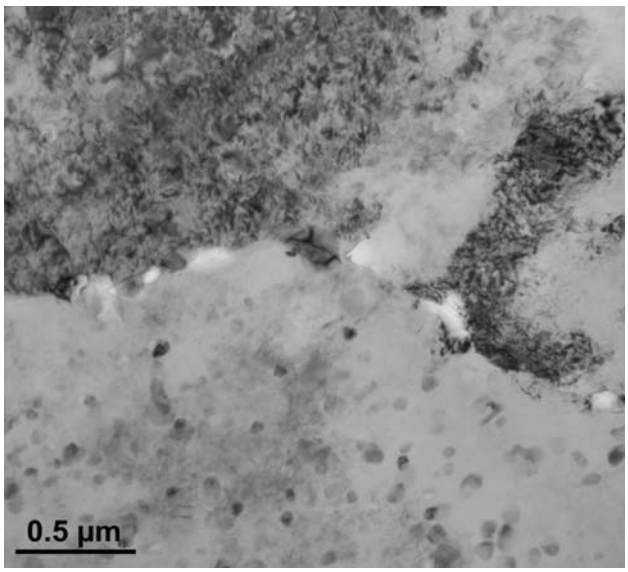

Fig. 11 TEM micrograph of voids occurring along grain boundary in Al 7075 spot weld produced using 2.5 mm/s plunge rate

associated with local melting in the stir zones of Al 7010 and Al 2024/SiC friction stir seam welds [50, 51].

The dissolution rate of melted droplets can be calculated using the methodology first developed by Reiso et al. [52] and Whelan [53]. Gerlich et al. [7] evaluated the non-isothermal dissolution kinetics of η phase particles when Al 7075 spot welds cool to room temperature following friction stir spot welding, see Fig. 13. Assuming a stir zone temperature of 475 °C, the radius of a spherical η particle decreases from 200 to 130 nm during the cooling cycle. Since η particles having dimensions around 80–100 nm are commonly observed in as-received Al 7075 base material, finding evidence supporting local melting in Al 7075 spot welds will be extremely difficult. The melted films shown

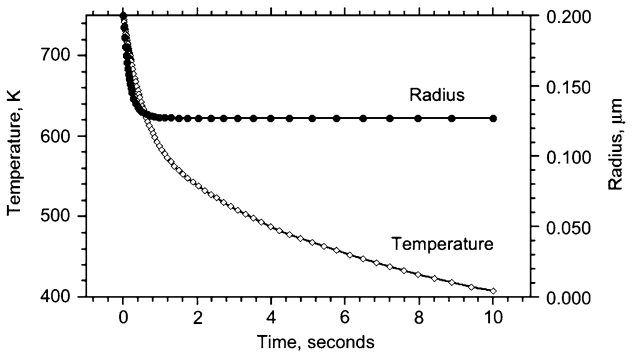

Fig. 13 Dissolution of η phase particles during cooling period following Al 7075 friction stir spot welding

in Fig. 12 are retained in Al 7075 spot welds precisely because measures are taken to prevent dissolution of melted eutectic material during the friction stir spot welding operation. An extremely short dwell time (0.05 s) and a high plunge rate are used in conjunction with quenching immediately following spot welding. Unless such steps are taken dissolution of particles in the high temperature stir zone and as the spot weld cools to room temperature will remove all evidence indicating that local melting has occurred during friction stir spot welding.

Conclusions

The present article has shown how local melting and tool slippage can be detected during friction stir spot welding of Al-alloy sections. Although the strain rate during welding can be estimated using the Zener–Hollomon relation, accurate stir zone temperature and grain size measurements are essential. The peak temperature within the stir zone is

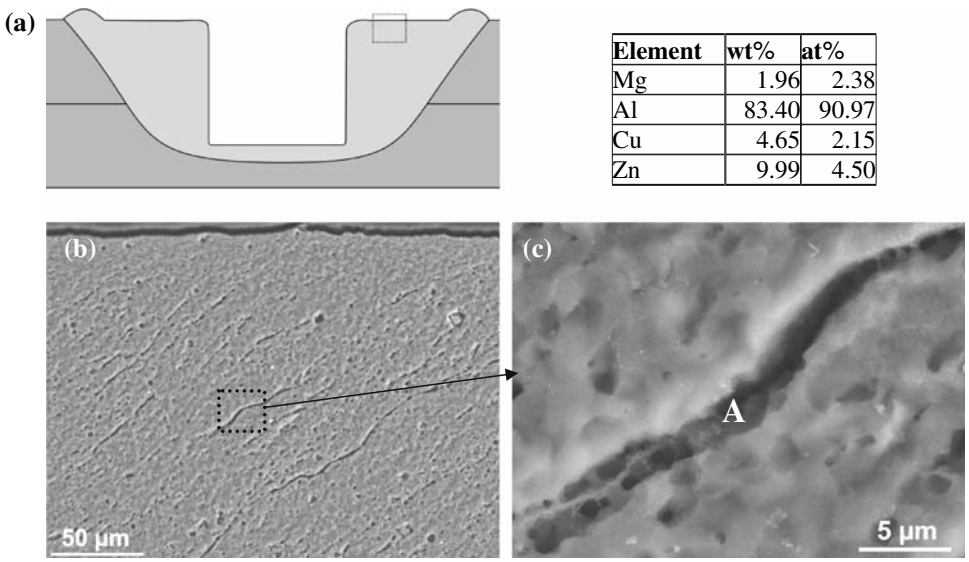

Element	wt%	at%
Mg	1.96	2.38
Al	83.40	90.97
Cu	4.65	2.15
Zn	9.99	4.50

Fig. 12 Melted films observed in an Al 7075 friction stir spot weld made using a plunge rate of 10 mm/s, a dwell time of 0.05 s and a tool rotation speed of 3,000 RPM. (**a**) Schematic of location in Al 7075 spot weld stir zone, (**b**) SEM micrograph showing the melted films, and (**c**) Detail showing the melted film and EDX chemical analysis at location A

ultimately limited by either the solidus of the alloy in question or by local melting of intermetallic particles, which spontaneously melt and facilitate tool slippage.

The drastic reduction in the estimated strain rate during friction stir spot welding results from spontaneous melting of second-phase particles contained in the as-received base material. Since local melted films dissolve rapidly in the high temperature stir zone and the spot welds cools to room temperature, evidence of local melting is only observed in spot welded joints produced using a combination of rapid quenching, high plunge rates, and extremely short dwell time settings.

Acknowledgement The authors wish to acknowledge financial support from the Natural Sciences and Engineering Research Council of Canada during this project.

References

1. Thomas WM, Nicholas ED, Needham JD, Murch MG, Templesmith P, Dawes CJ (1991/1995) G.B. Patent Application No. 9125978.8, Dec. 1991; U.S. Patent No. 5460317, Oct. 1995
2. Schilling C, Dos Santos J (2001) International Patent Publication No. WO 01/36144A1, May 25, 2001
3. Gerlich A, Su P, North TH (2005) J Mater Sci 40(24):6473
4. Sakano R, Murakami K, Yamashita K, Hyoie T, Fujimoto M, Inuzuka M, Nagao Y, Kashiki H (2001) Proc 7th Int Symp JWS 645
5. Lin P-C, Lin S-H, Pan J, Pan T, Nicholson JM, Garman MA (2004) SAE Technical Series, 2004-01-1330
6. Su P, Gerlich A, North TH (2005) SAE Technical Series, 2005-01-1255
7. Gerlich A, Avramovic-Cingara G, North TH (2006) Metall Trans A 37A:2773
8. Gerlich A, Su P, Yamamoto M, North TH (2007) J Mater Sci. doi:10.1007/s10853-006-1103-7
9. Su P, Gerlich A, North TH, Bendzsak GJ (2006) Sci Tech Weld Joining 11(2):163
10. Su P, Gerlich A, North TH, Bendzsak GJ (2006) SAE Technical Series, 2006-01-0971
11. Gerlich A, Su P, North TH (2005) Sci Tech Weld Joining 10(6):647
12. Gerlich A, Su P, North TH, Bendzsak GJ (2005) In: Nie JF, Barnett M (eds) Materials forum, vol 29, p 290
13. Gerlich A, Su P, North TH (2005) In: Neelameggham NR, Kaplan HI, Powell BR (eds) Magnesium technology 2005, TMS, p 383
14. North TH, Bendzsak GJ, Smith CB, Luan GH (2001) Proceedings of the 7th International Symposium on JWS. JWS, Japan, p 621
15. Gerlich A, Yamamoto M, North TH (2007) Metall Trans A accepted March 6, 2007
16. Dalle-Donne C, Braun B, Staniek G, Jung A, Kayser WA (1998) Materialwiss Werkstofftech 29:609
17. North TH, Bendzsak GJ, Smith CB (2000) Proceedings of 2nd international conference on friction stir welding. TWI, Gothenburg
18. Sato YS, Hwan S, Park C, Michiuchi M, Kokawa H (2004) Scr Mater 50(9):1233
19. Bendzsak GJ, North TH, Smith CB (2000) Proceedings of 2nd international conference on friction stir welding. TWI, Gothenburg
20. Droenen P-E, Ryum N (1994) Metall Trans A 25A:521
21. Bjørneklett B, Frigaard Ø, Grong Ø, Myhr OR, Midling OT (1999) Proceedings of 6th international conference on aluminium alloys. Toyoashi, Japan, p 1531
22. Li X-M, Starink MJ (2001) Mater Sci Technol 17:1324
23. Gerlich A, Su P, North TH, Bendzsak GJ (2006) Proceedings on friction stir welding colloquium. University of Graz, Austria, p 65
24. ASM metals handbook, 8th edn. (1961)
25. Su P, Gerlich A, North TH, Bendzsak GJ (2006) Metall Trans A accepted 2006
26. Aluminum: the corrosion resistant automotive material (2001) Publication AT7, The Aluminum Association
27. Davis JR (1993) Aluminum and aluminum alloys. ASM Intl., Materials Park
28. Bowden FP, Ridler KEW (1936) Proc R Soc London, Ser A 154(883):640
29. Bowden FP, Thomas PH (1954) Proc R Soc London, Ser A 223(1152):29
30. Gerlich A, Su P, Bendzsak GJ, North TH (2005) In: Jata KV, Mahoney MW, Mishra RS (eds) Friction stir welding and processing III. TMS, p 249
31. Quinn TFJ, Winer WO (1985) Wear 102:67
32. Yamamoto M, Su P, Gerlich A, North TH (2007) SAE Technical Series, 2007-01-1700
33. Song M, Kovacevic R (2002) Trans SME 621
34. Colegrove P, Shercliff H (2003) Sci Tech Weld Joining 8(5):360
35. Lambrakos SG, Fonda RW, Milewski JO, Mitchell JE (2003) Sci Tech Weld Joining 8(5):385
36. Mishin OV, Godfrey A, Östensson L (2006) Metall Trans A 37A:489
37. Humphreys FJ (2001) J Mater Sci 36:3833
38. Gerlich A, Cingara GA, North TH (2006) Mater Sci Forum 519–521:1107
39. Mcqueen HJ, Jonas JJ (1975) Treatise on materials science technology, vol 6. Academic Press, New York, p 393
40. Mcqueen HJ, Hocket JE (1970) Metall Trans A 1:2997
41. Avramovic-Cingara G, Mcqueen HJ (1994) Aluminium 70(3):214
42. Avramovic-Cingara G, Perovic DD, Mcqueen HJ (1996) Metall Mater Trans 27A:3478
43. Cerri E, Evangelista E, Forcellese A, Mcqueen HJ (1995) Mater Sci Eng A197:181
44. Sheppard T (1990) In: Chen CQ, Starke EA (eds) 2nd international conference on aluminum alloys—their physical and mechanical properties. International Academic Publisher, p 744
45. Mcqueen HJ (2003) Metall Trans A 33A:345
46. Sheppard T (1987) In: Leoben-Wien (ed) Proceedings of 8th light metal congress (8 Internationale Leichmetalltagung). p 301
47. Evangelista E, Mcqueen HJ, Bonetti E (1983) Deformation of multi-phase and particle containing materials. Risø National Laboratory, Roskilde, p 243
48. Pettersen T, Holmedal B, Nes E (2003) Metall Trans A 34A:2737
49. van Geertruyden WH, Misiolek WZ, Wang PT (2006) Mater Sci Eng A 419:105
50. Hassan KhAA, Prangnell PB, Norman AF, Price DA, Williams SW (2003) Sci Technol Weld Joining 8:257
51. Yan Y, Lui B, Zhang C (1998) Proceedings of 6th international conference on aluminium alloys. Toyoashi, Japan, p 1135
52. Reiso O, Øverlie H-G, Ryum N (1990) Metall Trans 21A:1689
53. Whelan MJ (1969) Met Sci J 3:95